



OPEN

Effect of the strain on spin-valley transport properties in MoS₂ superlattice

Farhad Sattari^{1,2}✉ & Soghra Mirershadi³

The effect of the strain on the spin and valley dependent transport properties, including the conductance and polarization, through a monolayer MoS₂ superlattice under Rashba spin-orbit coupling is theoretically investigated. It is found that the conductance strongly depends on the spin and valley degrees of freedom, and spin-inversion can be achieved by MoS₂ superlattice. Also, the spin and valley dependent conductance in a monolayer MoS₂ superlattice can be efficiently adjusted via strain and the number of the superlattice barriers. Moreover, it is demonstrated that both the magnitude and sign of the spin and valley polarization depend on the strain strength, the number of barriers, and electrostatic barrier height. Both full spin and valley polarized current (with 100% or -100% efficiency) can be realized in a MoS₂ superlattice under strain.

In recent years, two-dimensional (2D) materials have been attracted extensive interests due to their potential applications in various research fields. Graphene^{1,2} is currently the most important member of the 2D materials family. Since monolayer graphene is a gapless semiconductor, it has no useful applications in the semiconductor industry, logic, and spintronic devices. Within the 2D materials, monolayer molybdenum disulfide (MoS₂) was successfully synthesized via several experimental techniques³⁻⁷. Unlike graphene, the monolayer MoS₂ is a direct bandgap semiconductor with a tunable bandgap⁸. Due to the heavy transition-metal atoms, the monolayer MoS₂ has a strong spin-orbit coupling (SOC)⁹. Furthermore, in the monolayer MoS₂, in the Brillouin zone two inequivalent valleys (K and K') are separated by a large momentum¹⁰. Additionally, due to the symmetry breaking and large SOC in the monolayer MoS₂, it is possible to control and tune the spin and valley polarization properties in the monolayer MoS₂-based systems¹¹⁻¹³. Moreover, the monolayer MoS₂, in the presence of the Rashba spin-orbit coupling (RSOC), is a fascinating material for spintronics applications. In the monolayer MoS₂ the RSOC can easily be induced and tuned via an external electric field¹⁴ or a ferromagnetic exchange field¹⁵. On the other hand, the electronic, optical, and transport properties of the monolayer MoS₂ can be modulated by applying an external strain¹⁶⁻²⁰. The strain can be induced in the MoS₂ sheet by substrate²¹ or during the CVD growth²². In recent years, electron, spin and valley-dependent transport properties were reported extensively in monolayer MoS₂ structures, both experimentally and theoretically²³⁻³⁶. Fontana et al.²³ experimentally investigated the transport properties of the electron and hole in a gated MoS₂ Schottky barrier and found that in this structure, the source and drain electrodes' materials are essential keys in controlling the transport through the conduction or valence band. Rotjanapittayakul et al.²⁷ theoretically studied the magnetoresistance and spin injection in a MoS₂ junction, and demonstrated that a magnetoresistance and spin injection efficiency of the order of 300% and 80%, respectively, can be observed in a MoS₂-based tunnel junction. The effect of the Rashba spin-orbit interaction on the thermoelectric properties of monolayer MoS₂ nanoribbon is described in Ref.³¹, in which the authors presented that the magnitude and sign of Seebeck thermopower can be tuned by adjusting the structure's parameters. Besides, the superlattices structures³⁷ provide a new way for controlling the transport properties. Recently a great deal of attention has been addressed to the transport properties in superlattice-based 2D materials³⁸⁻⁵⁰. Yu and Liu⁴¹ studied the spin transport properties through monolayer and bilayer graphene superlattice. They showed that the monolayer and bilayer graphene superlattice with zigzag boundaries could be used for perfect spin-filtering. Zhang et al.⁴² demonstrated that a controllable spin and valley polarized current could be obtained in a silicene superlattice in the presence of the electric and magnetic field. The effect of the strain on the electronic properties in the MoS₂-WSe₂ moiré superlattice was investigated by Waters et al.⁴⁹. They found that in-plane strain and out-of-plane deformations significantly impact the MoS₂-WSe₂ moiré superlattice's

¹Department of Physics, Faculty of Sciences, University of Mohaghegh Ardabili, P.O. Box 179, Ardabil, Iran. ²Nanoscience and Nanotechnology Research Group, University of Mohaghegh Ardabili, Ardabil, Iran. ³Department of Engineering Sciences, Faculty of Advanced Technologies, University of Mohaghegh Ardabili, Namin, Iran. ✉email: f_sattari@uma.ac.ir

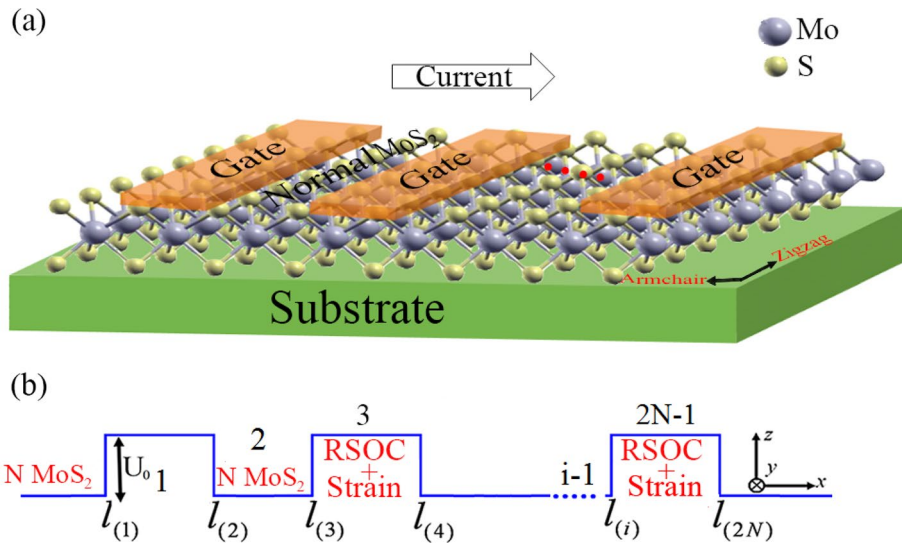


Figure 1. (a) Schematic representation of a monolayer MoS₂ superlattice under strain and RSOC. (b) Energy potential profile of MoS₂ superlattice with *N* electrostatic potential barrier.

electronic properties. In the present paper, we propose a monolayer MoS₂ superlattice in the presence of strain and RSOC in order to achieve a full spin and valley polarized current. We demonstrate that the spin and valley polarization’s magnitude and sign depend on the strain strength and the superlattice parameters. The results show that the conductance dependent on the spin and valley degrees of freedom and spin-inversion can be obtained by the MoS₂ superlattice.

Model and methods

In this work, we are interested in the spin- and valley-dependent transport properties in a MoS₂ superlattice with RSOC in the presence of a uniaxial strain. A series of metallic gate voltages on the top of monolayer MoS₂ with a suitable substrate can be used to get a monolayer MoS₂ superlattice in the presence of RSOC and strain. In our model, the RSOC region with a gate voltage and strain (barrier region) is separated by a normal monolayer MoS₂ (N MoS₂), in which there is no RSOC and strain (well region). The schematic of our proposed device structure is shown in Fig. 1. The growth direction of the superlattice is along the *x*-axis. We assume that the strain is applied in the armchair direction. The strain tensor, ϵ , can be written as follows²⁰

$$\epsilon = \epsilon \begin{pmatrix} \cos^2 \alpha - \mu \sin^2 \alpha & (1 + \mu) \cos \alpha \sin \alpha \\ (1 + \mu) \cos \alpha \sin \alpha & \sin^2 \alpha - \mu \cos^2 \alpha \end{pmatrix}, \quad (1)$$

where α is the angle between the *x*-axis and the direction of the strain. For the armchair direction strain $\alpha = 0$. ϵ is the strain strength and $\mu = 0.25$ is the Poisson’s ratio for the MoS₂⁵¹. In the considered structure, the low-energy effective Hamiltonian of the carriers near the K and K’ valleys can be written as:

$$\hat{H} = \hat{H}_0 + \hat{H}_{RSOC}, \quad (2)$$

with

$$\begin{aligned} \hat{H}_0 &= \hbar v_F U^\dagger(\alpha) [(\eta(1 - \lambda_x \epsilon) k_{s'(s)} \sigma_x + (1 - \lambda_y \epsilon) q_y \sigma_y)] U^\dagger(\alpha) + (\Delta + \eta s_z \lambda) \sigma_z + \eta s_z \lambda + V(x) \hat{I}, \\ \hat{H}_{RSOC} &= \lambda_R (s_y \otimes \sigma_x - s_x \otimes \sigma_y), \end{aligned} \quad (3)$$

$$V(x) = \begin{cases} U_0 & \text{in barrier} \\ 0 & \text{in well} \end{cases} \quad (4)$$

Here, $\hat{\sigma} = (\sigma_x, \sigma_y, \sigma_z)$ and $s = (s_x, s_y, s_z)$ are the Pauli matrices for the sublattice and the spin spaces, respectively. $v_F \approx 5.3 \times 10^5$ m/s denotes the Fermi velocity in a monolayer MoS₂, $\eta = +1/-1$ is the valley index ($\eta = 1$ for K and $\eta = -1$ for K’ valley) and $s_z = +1(-1)$ denotes the electron with the spin-up (down). $\Delta = 833$ meV is the energy gap¹² in the monolayer MoS₂, λ_R is RSOC strength and $\lambda = 37.5$ meV is the spin-splitting energy of the valence band caused by the spin-orbit coupling^{12,15}. U_0 displays the electrostatic potential barrier’s height, \hat{I} is a unitary matrix, $U(\alpha) = \text{diag}(1, e^{i\alpha})$ denotes the unitary matrix, which performs a rotation in the sublattice space⁵² and for the monolayer MoS₂ $\lambda_x = 2.2$ and $\lambda_y = -0.53$. Also, the longitudinal k_x ($k_{s'(s)}$) and the transverse k_y (q_y) components of the wave vectors in the N MoS₂ regions (in the ERSOC regions) with k ($k'_{s'(s)}$), respectively. k and $k'_{s'(s)}$ are given by:

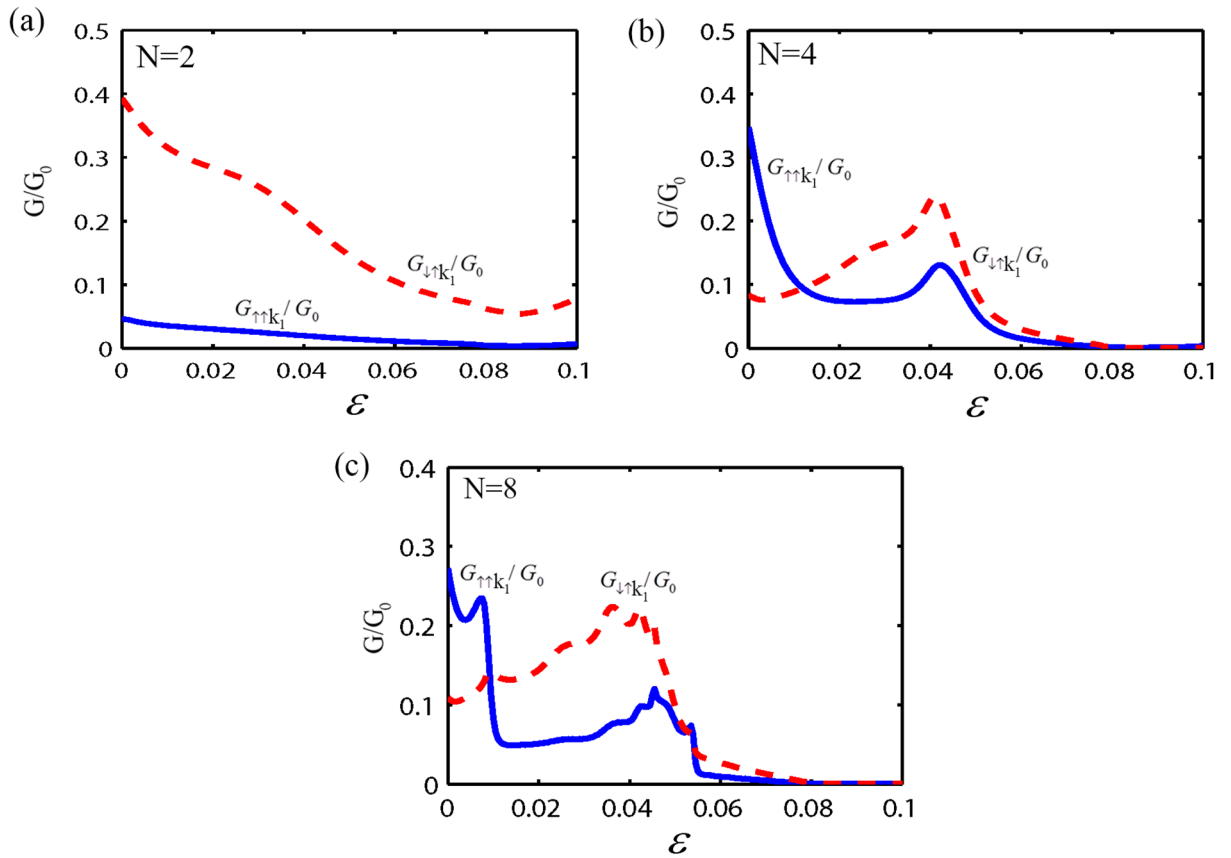


Figure 2. The spin dependent conductance for valley K_1 as a function of strain strength (ε), for fixed $E = 1.5\Delta$, $U_0 = 3.5\Delta$, $\lambda_R = 50$ meV, $k_{F0}b = 5$ and $k_{F0}w = 3$. For (a) two barrier, (b) four barriers, and (c) eight barriers structure.

$$k = ((\eta k_x)^2 + k_y^2) = \frac{1}{\hbar v_F} \sqrt{(E - 2\eta s_z \lambda + \Delta)(E - \Delta)}, \tag{5}$$

$$\begin{aligned} k'_{s'(s)} &= ((\eta k'_{s'(s)})^2 (1 - \lambda_x \varepsilon)^2 + q_y^2 (1 - \lambda_y \varepsilon)^2) \\ &= \sqrt{(E - \Delta - U_0)(E + \Delta - U_0 - 1(-1)2\eta\lambda - 1(-1)2\eta\lambda_R)/\hbar^2 v_F^2}. \end{aligned} \tag{6}$$

where, $k'_{s'(s)} = (1 - \lambda_x \varepsilon)^{-1} k'_{s'(s)} \cos \theta$ and $q_y = (1 - \lambda_y \varepsilon)^{-1} k'_{s'(s)} \sin \theta$. Let us now consider electrons with the angle of incidence of φ , spin s and energy E will go towards the monolayer MoS₂ superlattice from the left side. The spin and valley dependent wave function in the RSOC ($\psi_{s,\eta}^\pm$) and the normal ($\psi_{Ns,\eta}^\pm$) regions can be given by:

$$\begin{aligned} \psi_{N\uparrow\eta}^\pm &= ((\pm\eta k_x - ik_y), (E - \Delta)/\hbar v_F, 0, 0) e^{i(\pm k_x x + k_y y)} \times A, \\ \psi_{N\downarrow\eta}^\pm &= (0, 0, (\pm\eta k_x - ik_y), (E - \Delta)/\hbar v_F) e^{i(\pm k_x x + k_y y)} \times A, \\ A &= 1/\sqrt{2(|k_x|^2 + k_y^2 + ((E - \Delta)/\hbar v_F)^2)}, \end{aligned} \tag{7}$$

$$\begin{aligned} \psi_{\uparrow(\downarrow)\eta}^\pm &= \{[(\pm\eta k_{\uparrow(\downarrow)}) (1 - \lambda_x \varepsilon) - ((1 - \lambda_y \varepsilon) i q_y)], [E - \Delta - U_0]/\hbar v_F, -i \times 1(-1)[E - \Delta - U_0]/\hbar v_F, \\ &\quad -i \times 1(-1)(\pm\eta(k_{\uparrow(\downarrow)}(1 - \lambda_x \varepsilon) + ((1 - \lambda_y \varepsilon) i q_y))]\} \times e^{i(\pm k_{\uparrow(\downarrow)} x + k_y y)} D_{\uparrow(\downarrow)}, \\ D_{\uparrow(\downarrow)} &= 1/\sqrt{2(|k_{\uparrow(\downarrow)}|^2 \times (1 - \lambda_x \varepsilon)^2 + (q_y^2 \times (1 - \lambda_y \varepsilon)^2 + (E - \Delta - U_0)/\hbar v_F)^2)}, \\ k_{\uparrow(\downarrow)} &= \sqrt{(E - \Delta - U_0)(E + \Delta - U_0 - 2s_z \eta \lambda - 2s_z \eta \lambda_R)/\hbar^2 v_F^2 - (q_y^2 \times (1 - \lambda_y \varepsilon)^2)}. \end{aligned} \tag{8}$$

The spin and valley dependent transmission probability, $T_{s's\eta}$, (with the spin $s = \uparrow, \downarrow$ to be transmitted to the spin $s' = \uparrow, \downarrow$) through the monolayer MoS₂ superlattice with N electrostatic barriers can be obtained by applying the boundary conditions and using the transfer matrix approach^{54,55}. Then, the spin and valley dependent conductance of a monolayer MoS₂ superlattice under strain and RSOC is defined as⁵⁶:

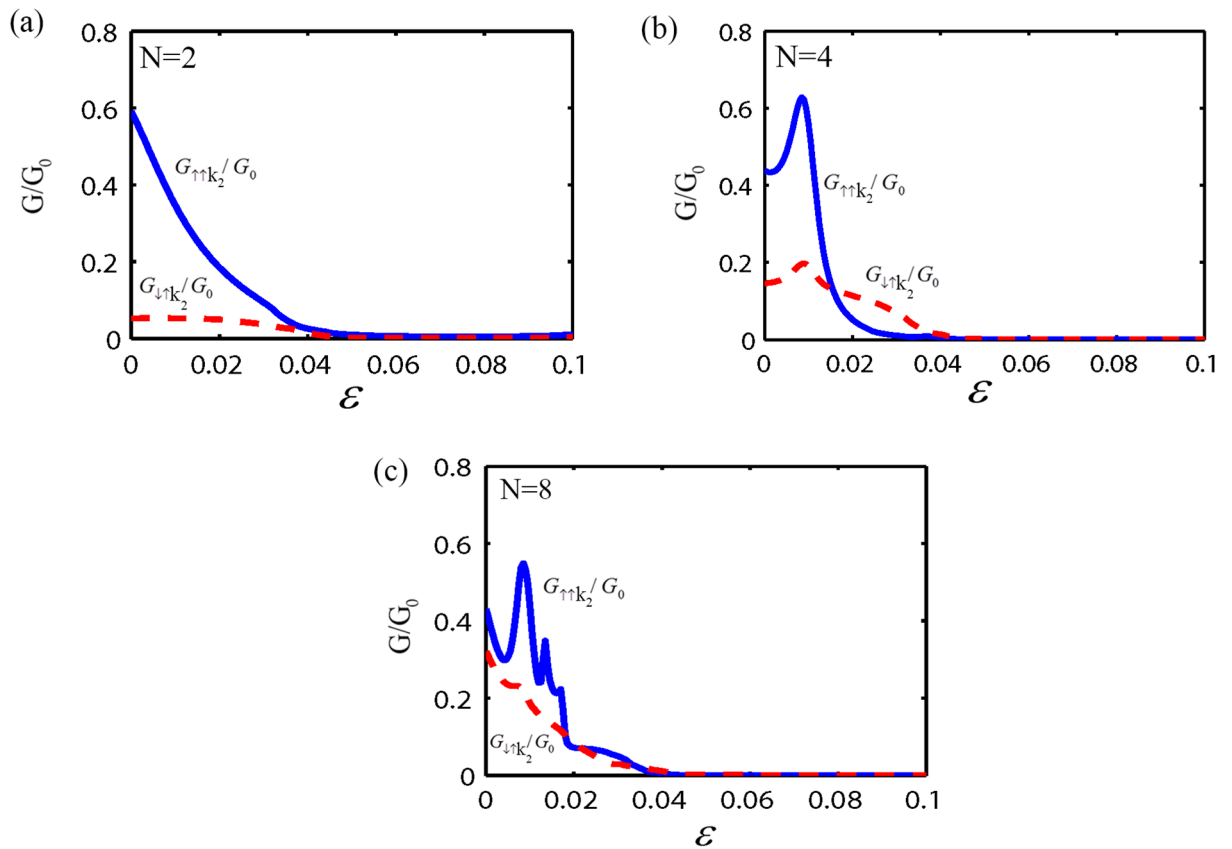


Figure 3. The spin dependent conductance for valley K_2 versus ε , for fixed $E = 1.5\Delta, U_0 = 3.5\Delta, \lambda_R = 50 \text{ meV}, k_{F0}b = 5$ and $k_{F0}w = 3$. For (a) two barrier, (b) four barriers, and (c) eight barriers structure.

$$G_{s's\eta} = G_0 \int_{-\pi/2}^{-\pi/2} T_{s's\eta}(\varphi) \cos(\varphi) d\varphi, \tag{9}$$

Finally, the spin and valley polarization can be calculated by⁵⁷:

$$P_S = \frac{G_{\uparrow\uparrow K_1} + G_{\uparrow\uparrow K_2} + G_{\downarrow\uparrow K_1} + G_{\uparrow\downarrow K_2} - G_{\downarrow\uparrow K_1} - G_{\downarrow\uparrow K_2} - G_{\downarrow\downarrow K_1} - G_{\downarrow\downarrow K_2}}{G_{\uparrow\uparrow K_1} + G_{\uparrow\uparrow K_2} + G_{\downarrow\uparrow K_1} + G_{\uparrow\downarrow K_2} + G_{\downarrow\uparrow K_1} + G_{\downarrow\uparrow K_2} + G_{\downarrow\downarrow K_1} + G_{\downarrow\downarrow K_2}}, \tag{10}$$

$$P_V = \frac{G_{\uparrow\uparrow K_1} + G_{\downarrow\uparrow K_1} + G_{\downarrow\downarrow K_1} + G_{\downarrow\uparrow K_1} - G_{\uparrow\uparrow K_2} - G_{\uparrow\downarrow K_2} - G_{\downarrow\downarrow K_2} - G_{\downarrow\uparrow K_2}}{G_{\uparrow\uparrow K_1} + G_{\downarrow\uparrow K_1} + G_{\downarrow\downarrow K_1} + G_{\downarrow\uparrow K_1} + G_{\uparrow\uparrow K_2} + G_{\uparrow\downarrow K_2} + G_{\downarrow\downarrow K_2} + G_{\downarrow\uparrow K_2}}. \tag{11}$$

Results and discussion

In the following, we consider the effect of both the strain and the RSOC on the spin and valley dependent conductance and polarization through the monolayer MoS₂ superlattice, as shown in Fig. 1. Here, we fix the parameters as; $E = 1.5\Delta, U_0 = 3.5\Delta, \lambda_R = 50 \text{ meV}$, the normalized barrier and the normal region width as $k_{F0}b = 5$ ($k_{F0} = E/\hbar v_F$) and $k_{F0}w = 3$, respectively. First, we investigate the valley and spin-dependent conductance as a function of the strain strength (ε) with a different number of electrostatic potential barriers. As shown in Fig. 2, the conductance for the valley K_1 depends on the spin degree of freedom and the number of the electrostatic barriers. Also for $N > 2$, the conductance without and with the spin-flip, shows an oscillatory behavior with respect to ε . Due to the strain and the normal regions' interface, more resonant peaks appear in the conductance by increasing the number of barriers in the superlattice. It is evident from Fig. 2 that the $G_{\uparrow\uparrow K_1}/G_0$ and $G_{\downarrow\uparrow K_1}/G_0$ decrease by increasing the strain strength. For a large strain and when number of superlattice barriers is big enough ($N \geq 4$), spin-dependent conductance tends to zero. This is due to the evanescent states in the strain region. According to Fig. 2a, it is clear that for $\varepsilon \geq 0.08$, the value of $G_{\uparrow\uparrow K_1}/G_0 = 0$ and $G_{\downarrow\uparrow K_1}/G_0 \neq 0$. In other words, electrons could transmit through the monolayer MoS₂ superlattice only with spin-flip. In this case the spin state of outgoing electrons were inverted by using monolayer MoS₂ superlattice. So, the monolayer MoS₂ superlattice acts as a spin inverter. The conductance for the valley K_2 is presented in Fig. 3. It is observed that for $\varepsilon > 0.04$ the spin-dependent conductance, without and with spin-flip, in a monolayer MoS₂ superlattice has a zero value due to the evanescent waves. This leads to a gap in the spin-dependent conductance with respect to the

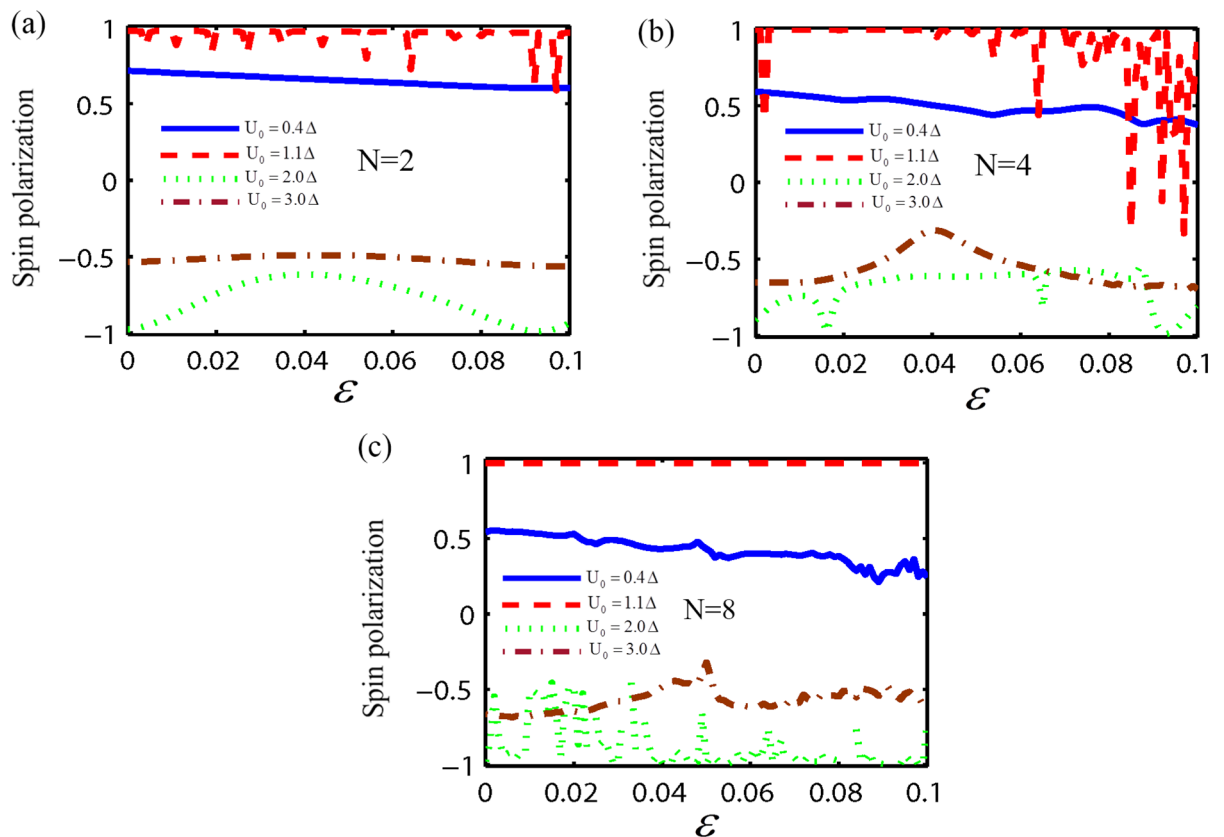


Figure 4. The spin polarization as a function of ε with several values of the height of the electrostatic potential barrier, for fixed $E = 1.5\Delta$, $\lambda_R = 50$ meV, $k_{F0}b = 5$ and $k_{F0}w = 3$. For (a) two barrier, (b) four barriers, and (c) eight barriers structure.

strain strength. Furthermore, when $\varepsilon < 0.04$, the conductance depends on the spin orientation of the electrons, and for $N > 2$, $G_{\uparrow\uparrow K_2}/G_0$ and $G_{\downarrow\uparrow K_2}/G_0$ shows an oscillatory behavior with ε , due to the propagating states in the strain region. According to Figs. 2 and 3, in a monolayer MoS₂ superlattice, the conductance depends on both the spin and valley degrees of freedom. Thus, the spin and valley dependent conductance in a monolayer MoS₂ superlattice can easily be adjusted by the strain. The other motivation of this paper is the calculation of the valley and spin polarization in a monolayer MoS₂ superlattice under strain and RSOC. For this purpose, we first plot the spin polarization versus the strain strength, with a different number of barriers and several values of the height of the electrostatic potential barrier, in Fig. 4. According to Fig. 4, at first, by increasing the potential barrier's height, the spin polarization rises and reaches a maximum value. With the further increment of the electrostatic barrier height, the sign of the spin polarization is changed. In other words, the spin polarization shows great sensitivity to the number of electrostatic barriers and the barrier height, also the magnitude and sign of the spin polarization can be effectively manipulated by adjusting the number of barriers, the height of the electrostatic barrier, and the strain. The valley polarization is plotted in Fig. 5 as a function of the strain strength with a different number of barriers and several barrier height values. As shown in Fig. 5, the valley polarization has an oscillating evolution with the strain. Also, due to the oscillatory behavior of the conductance in terms of the barrier's height, the spin and valley dependent polarization will also show such behavior as a function of the barrier's height. Furthermore, it is seen from Fig. 5 that the valley polarization oscillates from -1 to 1 as ε varies. By increasing the number of barriers in the MoS₂ more resonant peaks appear in the valley and spin dependent polarization superlattice, due to the strain and the normal regions' interface. Consequently, the magnitude and the direction of the valley polarization can be tuned by the strain in a MoS₂ superlattice. A fully valley polarized current occurs when the value of valley polarization is at its maximum values (1 or -1). In this case, only the carriers from one valley (K or K') will contribute to the conduction. Similar to the spin polarization, the number of the barriers and the barrier height are essential parameter in controlling the valley dependent transport properties in a monolayer MoS₂ superlattice. These results imply that the MoS₂ superlattice are excellent candidates for future straintronic and spintronic applications.

Conclusion

In summary, we have investigated the spin and valley-dependent transport properties in a monolayer MoS₂ superlattice under uniaxial strain and RSOC. We found that the strain has a significant effect on the spin and valley dependent conductance, without and with the spin-flip. Furthermore, we showed that the valley and spin dependent conductance have a gap regarding the strain, which allows the valley and spin conductance to

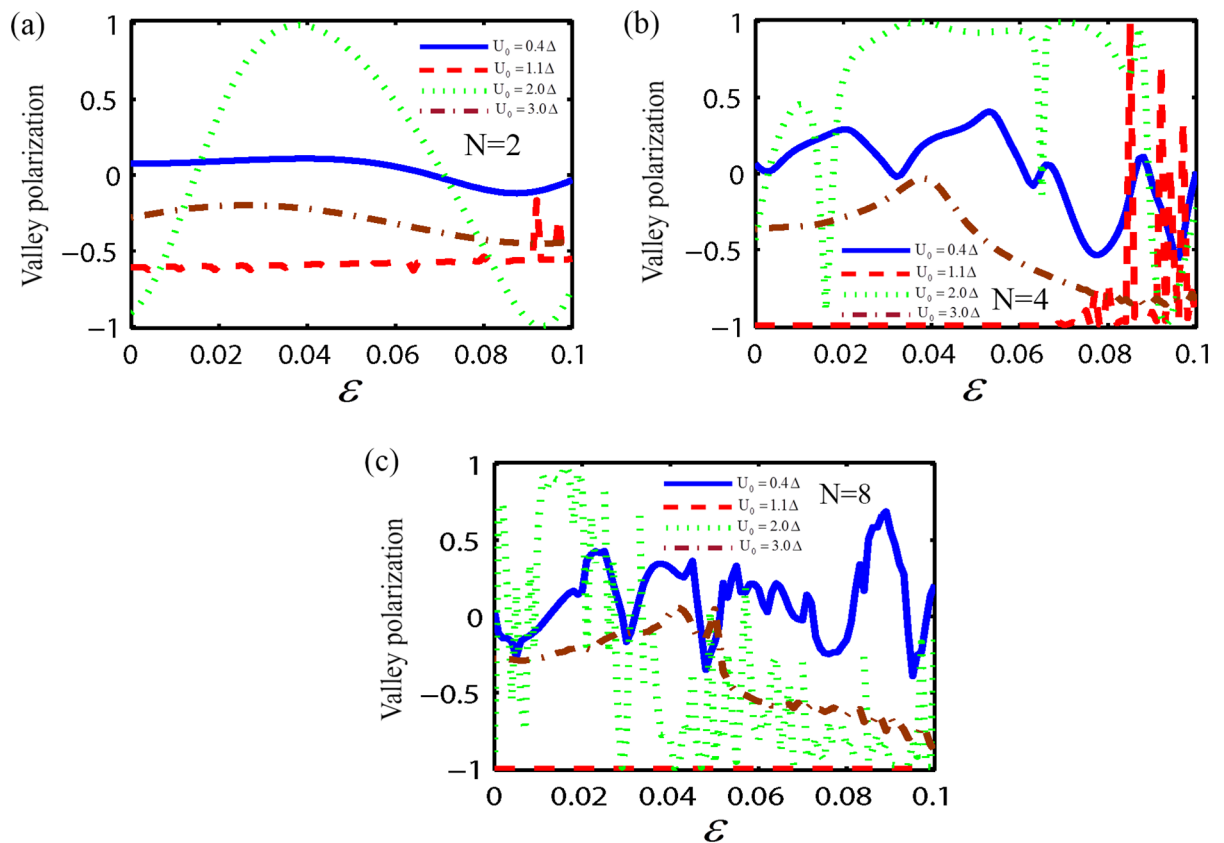


Figure 5. Dependence on the ε of the valley spin polarization with several values of the height of the electrostatic potential barrier, for fixed $E = 1.5\Delta$, $\lambda_R = 50$ meV, $k_{F0}b = 5$ and for (a) two barrier, (b) four barriers, and (c) eight barriers structure.

have an on/off switching effect. More importantly, we produced both full spin and valley polarized current in a monolayer MoS₂ superlattice under an armchair strain. Meanwhile, the magnitude and the direction of the valley and spin polarization can be tuned by strain, the number of electrostatic barriers, and barrier height. Our calculations indicated that the transport properties in a MoS₂ superlattice under RSO could be efficiently controlled mechanically.

Received: 6 March 2021; Accepted: 23 August 2021

Published online: 02 September 2021

References

- Novoselov, K. S. *et al.* Electric field effect in atomically thin carbon films. *Science* **306**, 666–669 (2004).
- Gaim, A. K. & Novoselov, K. S. The rise of graphene. *Nat. Mater.* **6**, 183–191 (2007).
- Lee, Y. H. *et al.* Synthesis of large-area MoS₂ atomic layers with chemical vapor deposition. *Adv. Mater.* **24**, 2320–2325 (2012).
- Kong, D. *et al.* Synthesis of MoS₂ and MoSe₂ films with vertically aligned layers. *Nano Lett.* **13**, 1341–1347 (2013).
- Li, H., Wu, H., Yuan, S. & Qian, H. Synthesis and characterization of vertically standing MoS₂ nanosheets. *Sci. Rep.* **6**, 21171 (2016).
- Sharma, M., Singh, A. & Singh, R. Monolayer MoS₂ transferred on arbitrary substrates for potential use in flexible electronics. *ACS Appl. Nano Mater.* **3**, 4445–4453 (2020).
- Park, S. *et al.* Layer-selective synthesis of MoS₂ and WS₂ structures under ambient conditions for customized electronics. *ACS Nano* **14**, 8485–8494 (2020).
- Mak, K. F., Lee, C., Hone, J., Shan, J. & Heinz, T. F. Atomically thin MoS₂: A new direct-gap semiconductor. *Phys. Rev. Lett.* **105**, 136805 (2010).
- Zhu, Z. Y., Cheng, Y. C. & Schwingenschlögl, U. Giant spin-orbit-induced spin splitting in two-dimensional transition-metal dichalcogenide semiconductors. *Phys. Rev. B* **84**, 153402 (2011).
- Li, Z. & Carbotte, J. P. Longitudinal and spin-valley Hall optical conductivity in single layer MoS₂. *Phys. Rev. B* **86**, 205425 (2012).
- Mak, K. F., He, K., Shan, J. & Heinz, T. F. Control of valley polarization in monolayer MoS₂ by optical helicity. *Nat. Nanotech.* **7**, 494 (2012).
- Xiao, D. *et al.* Coupled spin and valley physics in monolayers of MoS₂ and other group-VI dichalcogenides. *Phys. Rev. Lett.* **108**, 196802 (2012).
- Lu, H. Z., Yao, W., Xiao, D. & Shen, S. Q. Intervalley scattering and localization behaviors of spin-valley coupled dirac fermions. *Phys. Rev. Lett.* **110**, 016806 (2013).
- Shao, Q. *et al.* Strong Rashba-Edelstein effect-induced spin-orbit torques in monolayer transition metal dichalcogenide/ferromagnet bilayers. *Nano Lett.* **16**, 7514–7520 (2016).
- Xiao, Y. M., Xu, W., Van Duppen, B. & Peeters, F. M. Infrared to terahertz optical conductivity of *n*-type and *p*-type monolayer MoS₂ in the presence of Rashba spin-orbit coupling. *Phys. Rev. B* **94**, 155432 (2016).

16. Scalise, E., Houssa, M., Pourtois, G., Afanas'ev, V. & Stesmans, A. Strain-induced semiconductor to metal transition in the two-dimensional honeycomb structure of MoS₂. *Nano Res.* **5**, 43–48 (2012).
17. Johari, P. & Shenoy, V. B. Tuning the electronic properties of semiconducting transition metal dichalcogenides by applying mechanical strains. *ACS Nano* **6**, 5449–5456 (2012).
18. Chen, S. F. & Wu, Y. R. Electronic properties of MoS₂ nanoribbon with strain using tight-binding method. *Phys. Status Solidi B* **254**, 1600565 (2017).
19. Liu, R. *et al.* Piezotronic spin and valley transistors based on monolayer MoS₂. *Nano Energy* **72**, 104678 (2020).
20. Li, L., Castro, E. V. & Sacramento, P. D. Strain induced topological phase transition at zigzag edges of monolayer transition-metal dichalcogenides. *Phys. Rev. B* **94**, 195419 (2016).
21. Castellanos-Gomez, A. *et al.* Local strain engineering in atomically thin MoS₂. *Nano Lett.* **13**, 5361–5366 (2013).
22. Luo, S., Cullen, C. P., Guo, G., Zhong, J. & Duesberg, G. S. Investigation of growth-induced strain in monolayer MoS₂ grown by chemical vapor deposition. *Appl. Surf. Sci.* **508**, 145126 (2020).
23. Fontana, M. *et al.* Electron-hole transport and photovoltaic effect in gated MoS₂ Schottky junctions. *Sci. Rep.* **3**, 1634 (2013).
24. Sun, J. F. & Cheng, F. Spin and valley transport in monolayers of MoS₂. *J. Appl. Phys.* **115**, 133703 (2014).
25. Chang, T. R., Lin, H., Jeng, H. T. & Bansil, A. Thickness dependence of spin polarization and electronic structure of ultra-thin films of MoS₂ and related transition-metal dichalcogenides. *Sci. Rep.* **4**, 6270 (2014).
26. Pawłowski, J., Żebrowski, D. & Bednarek, S. Valley qubit in a gated monolayer quantum dot. *Phys. Rev. B* **97**, 155412 (2018).
27. Rotjanapittayakul, W., Pijitrojana, W., Archer, T., Sanvito, S. & Prasongkit, J. Spin injection and magnetoresistance in MoS₂-based tunnel junctions using Fe₃Si Heusler alloy electrodes. *Sci. Rep.* **8**, 4779 (2018).
28. Riccardo, P. *et al.* Interactions and magnetotransport through spin-valley coupled Landau levels in monolayer MoS₂. *Phys. Rev. Lett.* **121**, 247701 (2018).
29. Roch, J. G. *et al.* Spin-polarized electrons in monolayer MoS₂. *Nat. Nanotechnol.* **14**, 432–436 (2019).
30. Lin, J. *et al.* Determining interaction enhanced valley susceptibility in spin-valley-locked MoS₂. *Nano Lett.* **19**, 1736–1742 (2019).
31. Shokri, A. & Salami, N. Thermoelectric properties in monolayer MoS₂ nanoribbons with Rashba spin-orbit interaction. *J. Mater. Sci.* **54**, 467–482 (2019).
32. Sattari, F. & Mirershadi, S. Spin and valley dependent transport in a monolayer MoS₂ superlattice with extrinsic Rashba spin-orbit interaction. *J. Magn. Magn. Mater.* **514**, 167256 (2020).
33. Gut, D., Prokop, M., Sticlet, D. & Nowak, M. P. Valley polarized current and resonant electronic transport in a nonuniform MoS₂ zigzag nanoribbon. *Phys. Rev. B* **101**, 085425 (2020).
34. Chen, W., Zhou, X., Liu, P., Xiao, X. & Zhou, G. Effect of trigonal warping on the Berry curvature and valley/spin Hall effects in monolayer MoS₂. *Phys. Lett. A* **384**, 126344 (2020).
35. Kim, T., Fan, S., Lee, S., Joo, M. K. & Lee, Y. H. High-mobility junction field-effect transistor via graphene/MoS₂ heterointerface. *Sci. Rep.* **10**, 13101 (2020).
36. Wang, K. *et al.* Polarization-driven edge-state transport in transition-metal dichalcogenides. *Phys. Rev. Appl.* **13**, 054074 (2020).
37. Esaki, L. & Tsu, R. Superlattice and negative differential conductivity in semiconductors. *IBM J. Res. Dev.* **14**, 61 (1970).
38. Park, C. H. *et al.* Anisotropic behaviors of massless Dirac fermions in graphene under periodic potential. *Nat. Phys.* **4**, 213 (2008).
39. Li, X., Zhang, F., Niu, Q. & Feng, J. Superlattice valley engineering for designer topological insulators. *Sci. Rep.* **4**, 6397 (2014).
40. Niu, Z. P., Zhang, Y. M. & Dongh, S. Enhanced valley-resolved thermoelectric transport in a magnetic silicene superlattice. *New J. Phys.* **17**, 073026 (2015).
41. Yu, H. & Liu, J. F. Perfect Spin-filtering in graphene monolayer-bilayer superlattice with zigzag boundaries. *Sci. Rep.* **6**, 25361 (2016).
42. Zhang, Q., Chan, K. S. & Li, J. Electrically controllable sudden reversals in spin and valley polarization in silicene. *Sci. Rep.* **6**, 33701 (2016).
43. Briones-Torres, J. A. & Rodríguez-Vargas, I. Fano resonances in bilayer graphene superlattices. *Sci. Rep.* **7**, 16708 (2017).
44. Zhang, Y., Kim, Y., Gilbert, M. J. & Mason, N. Magnetotransport in a strain superlattice of graphene. *Appl. Phys. Lett.* **115**, 143508 (2019).
45. Huber, R. *et al.* Gate-tunable two-dimensional superlattices in graphene. *Nano Lett.* **20**, 8046–8052 (2020).
46. Chen, H. *et al.* Tunable photoelectronic properties of hydrogenated silicene/halogenated-silicene superlattices for water splitting. *J. Appl. Phys.* **127**, 084301 (2020).
47. Wang, J. J., Liu, S., Wang, J. & Liu, J. F. Valley supercurrent in the Kekulé graphene superlattice heterojunction. *Phys. Rev. B* **101**, 245428 (2020).
48. Kraft, R. *et al.* Anomalous cyclotron motion in graphene superlattice cavities. *Phys. Rev. Lett.* **125**, 217701 (2020).
49. Waters, D. *et al.* Flat bands and mechanical deformation effects in the moiré superlattice of MoS₂-WSe₂ heterobilayers. *ACS Nano* **14**, 7564–7573 (2020).
50. Tavakoli, F., Faizabadi, E., Elahi, S. M. & Hantehzadeh, M. Spin-polarization and spin-flip through a monolayer MoS₂ superlattice via the Rashba effect. *J. Comput. Electron* **20**, 126–134 (2021).
51. Guzman, D. M. & Strachan, A. Role of strain on electronic and mechanical response of semiconducting transition-metal dichalcogenide monolayers: An ab-initio study. *J. Appl. Phys.* **115**, 243701 (2014).
52. Chen, X., Deng, Z. Y. & Ban, Y. Delay time and Hartman effect in strain engineered graphene. *J. Appl. Phys.* **115**, 173703 (2014).
53. Yarmohammadi, M. The effects of strain on DC transverse and spin-valley Hall conductivity of ferromagnetic MoS₂ and silicene. *J. Magn. Magn. Mater.* **426**, 621–628 (2017).
54. Bai, C. & Zhang, X. Klein paradox and resonant tunneling in a graphene superlattice. *Phys. Rev. B* **76**, 075430 (2007).
55. Abedpour, N., Esmailpour, A., Asgari, R. & Tabar, M. R. R. Conductance of a disordered graphene superlattice. *Phys. Rev. B* **79**, 165412 (2009).
56. Büttiker, M. Four-terminal phase-coherent conductance. *Phys. Rev. Lett.* **57**, 1761 (1986).
57. Li, H., Shao, J., Yao, D. & Yang, G. Gate-voltage-controlled spin and valley polarization transport in a normal/ferromagnetic/normal MoS₂ junction. *ACS Appl. Mater. Interfaces* **6**, 1759–1764 (2014).

Author contributions

All authors conceived the study. F.S. performed the numerical calculations. S.M. wrote the main manuscript text. All authors have contributed in analyzing the results and preparing the manuscript.

Competing interests

The authors declare no competing interests.

Additional information

Correspondence and requests for materials should be addressed to F.S.

Reprints and permissions information is available at www.nature.com/reprints.

Publisher's note Springer Nature remains neutral with regard to jurisdictional claims in published maps and institutional affiliations.



Open Access This article is licensed under a Creative Commons Attribution 4.0 International License, which permits use, sharing, adaptation, distribution and reproduction in any medium or format, as long as you give appropriate credit to the original author(s) and the source, provide a link to the Creative Commons licence, and indicate if changes were made. The images or other third party material in this article are included in the article's Creative Commons licence, unless indicated otherwise in a credit line to the material. If material is not included in the article's Creative Commons licence and your intended use is not permitted by statutory regulation or exceeds the permitted use, you will need to obtain permission directly from the copyright holder. To view a copy of this licence, visit <http://creativecommons.org/licenses/by/4.0/>.

© The Author(s) 2021